Quantitative Measurements of Polymer Chain-End Edge Dislocation Strain Fields by High Resolution Electron Microscopy

Patricia M. Wilson† and David C. Martin*

Materials Science and Engineering, The University of Michigan, 2022 H. H. Dow Building, Ann Arbor, Michigan 48109-2136

Received May 16, 1995; Revised Manuscript Received October 16, 1995⊗

ABSTRACT: The strain fields around chain-end edge dislocations in poly(diacetylene) crystals were analyzed by high resolution electron microscopy (HREM). Experimental measurements of the tilt of the polymer chain axis as a function of azimuthal angle ϕ at a constant radius r from the dislocation core were compared to theoretical predictions. The shear deformation was localized in parabolic regions parallel to the Burger's vector **b** near the chain end. For an edge dislocation in the poly(diacetylene) 1,6-di(*N*-carbazolyl)-2,4-hexadiyne (DCHD) with a Burger's vector of **b** = 3a/2 [100] (2.4 nm), we found a tilt distortion of ±6° at 12 nm from the core. A parameter W was introduced to describe the anisotropy of the compliance matrix with respect to the chain direction. A parameter of $W = 3.5$ was needed to fit the measured tilt deformation with anisotropic linear elastic dislocation theory. We also found that the theory of distortions near dislocations in columnar liquid crystals could closely predict our experimental observations. A value of 0.8 nm (the interchain spacing) for the characteristic length, λ_3, was the best fit for the columnar liquid crystal solution. This analysis reveals similarities between the elasticity of anisotropic crystals and liquid crystals.

Introduction

While the study of defects in crystalline inorganic materials is well-developed, the understanding of defects in polymers and organic solids is still in its infancy. In molecular systems, it is necessary to consider the role of covalent bonds on defect structure and mobility. Classification schemes for describing defects in polymers have been presented by Wunderlich.[1,2] Point defects specific to crystalline polymers have been discussed by Reneker and Mazur.[3,4] The structure and properties of defects in polymer solids have been the subject of a recent review.[5] As ordered polymers continue to attract interest as the active components of optical and electronic devices, the rational manipulation of defect structure and properties should provide an additional means for controlling macroscopic properties.

In molecular systems, defects which disrupt the orientation or connectivity of covalent bonds are expected to be particularly important in determining properties.[6] Here, we examine the microstructure near the core of chain-end edge dislocations in extended-chain poly(diacetylenes). By measuring the distortions near the defects at high resolution, we were able to obtain information about the anisotropic elasticity of the polymer crystal.

Background

Poly(diacetylenes) are prepared in a solid-state reaction from crystals of a precursor monomer. The topochemical polymerization of diacetylenes leads to a single crystal morphology in which the chains are fully extended. Diacetylenes are one-dimensional semiconductors because of the conjugation along the extended chain backbone and the large distance (∼0.7−0.8 nm) between molecules which inhibits lateral charge carrier hopping. The electronic structure changes near defects have implications for device fabrication. Traps would be created at dislocations formed by chain ends where the conjugation is disrupted. Bending of the backbone could also disturb the conjugation length. Hone and Singh[6] have examined the implications of structural defects on the nonlinear optical susceptibility of diacetylenes. They looked at the effect of a random distribution of bond breaking defects on the third-order nonlinear susceptibility (χ^3) using a tight binding (Huckel) model. They predicted that the susceptibility would decrease as the density of π-bond breaking defects increased.

Experiments measuring the photocurrent through manufactured poly(diacetylene) bicrystals provide insight about the behavior of chain-end dislocation defects at grain boundaries as deep traps.[7] With increasing misorientation between the crystals, the efficiency of charge carrier transport decreases. The information from these experiments provides a basis for the design and optimization of optoelectronically active polymer devices.

It is expected that chain end dislocations in diacetylenes form in the monomer during crystallization from the solvent. The subsequent polymerization would freeze the dislocations into the polymer lattice. Chain-end dislocations in polymers should be sessile because their motion would require covalent bonds to be bent or broken. This is in contrast to the **b** = [001] edge dislocations parallel to the polymer chain axis.[8,9] Dislocations with a Burger's vector parallel to the chain have a lower barrier to movement by glide parallel to **b** and would be glissile. Similar glissile dislocations have been described in polyethylene.[10] Their movement is the mechanism that explains shearing of the lamella when a crystal settles on a substrate step or particle. Young[11] and Crist[12] have described yield in semicrystalline polymers by similar dislocation-mediated deformation mechanisms.

Dislocations in the poly(diacetylene) poly(toluene sulfonate) (pTS) have been imaged by dark-field transmission electron microscopy (TEM).[8] The strain fields

* To whom correspondence should be addressed.
† Present address: Foster-Miller, Inc., 195 Bear Hill Rd., Waltham, MA 02154-1196.
⊗ Abstract published in *Advance ACS Abstracts,* December 15, 1995.

0024-9297/96/2229-0842$12.00/0

around the dislocations were estimated from TEM dark field image contrast to be larger than would be expected for an isotropic material. The strain fields in pTS were extended over 30 monomer units (along the [001] direction) for an edge dislocation with a Burger's vector parallel to the chain axis. However, the limited resolution of the dark-field technique did not make it possible to determine the local distortions near an individual defect. A single chain-end dislocation in DCHD was imaged directly by high resolution electron microscopy (HREM) by Read and Young,[13] but no attempt was made to quantitatively examine the nature or extent of the distortions near the dislocation core.

Recent advances have demonstrated the utility of HREM imaging techniques for examining defect structures in ordered polymers.[14−17] Here, we show how HREM can be used to quantify the local deformation field around individual dislocations. By measuring the magnitude of the distortions near the defect, it is possible to extract information about the anisotropic elasticity of the polymer. While our specific interest here is in chain-end edge dislocations in crystalline polymers, it may also be possible to adapt this approach to examine dislocations in liquid crystalline or microphase separated systems.

Previous studies have taken advantage of quantitative measurements of microstructure to extract information about the physical behavior of polymers in the condensed state. Hudson and Thomas[18] presented a technique for estimating the bend-to-splay elastic anisotropy in thermotropic liquid crystalline polymers (TLCP's) from transmission electron microscope images of the director field near the core of a disclination. Hudson et al.[19] extended this analysis to examine changes in the elastic response of the polymer as a function of the distance from the disclination core. The elastic anisotropy of thermotropic polyesters was found to be different within several molecular lengths of the core. The sign and magnitude of this effect were a function of the chemical composition of the polymer, evidently due to differences in the rigidity of the backbone and the subsequent ability to form hairpin defects. Ding and Thomas[20] were able to estimate the elastic anisotropy in TLCP's by measuring the director orientation across Néel inversion walls.

Quantitative studies of distortions in amorphous polymers can be obtained by using a suitable reference frame. Corleto et al.[21] used scanning electron microscopy to reveal the displacement of a grid of fine dots placed on the surface of a cross-linked epoxy sample near a crack tip. The polymer samples were found to exhibit intense plastic deformation around the crack (local strains ∼37%), despite the fact that the macroscopic elongation was small (less than 5%).

Strain field information has been extracted from high resolution images of dislocations in inorganic materals such as silicon.[22,23] Computational Fourier transform deformation analysis was used to extract a Moiré pattern from a digitized HREM image by filtering the optical diffractogram and calculating the inverse Fourier transform. The Moiré pattern was then used to derive the displacement gradient from which the strain fields were calculated.[22,23] The strain fields from a defect image of a dislocation in silicon resembled theoretical predictions obtained from linear isotropic elasticity theory. However, this work failed to take into account artifacts which may arise due to Fourier filtering the image. Pradere and Thomas[24] showed that, by changing the size of the window used to Fourier filter a dislocation dipole image in poly(*p*-xylylene) (PPX), drastically different images could be produced in which the defect information could vanish or the apparent bending of the associated lattice planes was increased.

HREM lattice images of crystalline polymers make it possible to determine the local tilt of the chain axis relative to the direction of the electron beam. Here we will show that the chain tilt is directly related to the shear strain around the dislocation. The experimentally determined strain field near chain-end edge dislocations will be examined and compared to theories of this deformation. Polymer crystals exhibit anisotropic crystalline moduli due to the one-dimensional covalent bonding and relatively weak van der Waals or hydrogen bonding between molecules. Hence, it is necessary to use anisotropic elasticity theory to describe the distortions near dislocations in polymer crystals.[25] Peterson and Lindenmeyer[26] recognized the need to analyze screw dislocations in orthorhombic polyethylene using anisotropic elasticity theory. Their analysis of the contrast of dislocations in TEM using two-beam electron imaging provided an estimate of the anisotropy of the elastic stiffness moduli, c_{66} and c_{55}. Their study relied on the kinematic extinction thickness in polyethylene as a parameter to match the crystal anisotropy to the image contrast. However, it is known that dynamical scattering effects can be particularly important for determining extinction distances in electron diffraction even for thin organic samples.[27]

Liquid crystalline materials can also exhibit dislocations in both layered (smectic) and rod-like (columnar) structures.[28] A columnar phase has two-dimensional positional order in the transverse direction but no axial correlations between columns.[29] In a polymer crystal the fact that the modulus in the chain direction is considerably higher than the transverse modulus reduces the relative influence of lateral correlations between chains. It will be shown in this paper that as the anisotropy of the crystal moduli is increased, the strain around a polymer chain-end edge dislocation predicted by linear anisotropic elasticity becomes similar to that of a columnar liquid crystal. The distortions due to shear interactions between columns become smaller in anisotropic than in isotropic crystals and vanish completely in columnar liquid crystals.

Experimental Section

Analysis of Dislocation Images. HREM images of chain end dislocations in 1,6-di(*N*-carbazolyl)-2,4-hexadiyne (DCHD) poly(diacetylene) crystals were obtained on a JEOL 4000 EX at 400 kV by low dose methods.[30] The orientation and spacings of the lattice images were calibrated by shadowing with gold. The fringes obtained were primarily those from the (*hk*0) family of planes parallel to the chain axis. Multislice simulations of HREM image contrast using the crystal structure of DCHD poly(diacetylene) (space group $P2_1/c$, $a = 1.74$ nm, $b = 1.29$ nm, $c = 0.49$ nm, $\gamma = 108.3$)[31] confirm that the (*hk*0) fringes are parallel to the chain axis ([001]).

The deformation field was mapped by measuring the local orientation of the molecular director around the dislocation. The data was analyzed by plotting the chain orientation θ as a function of azimuthal angle ϕ at a fixed radius r. The measured tilt was relative to the chain axis of a perfect crystal, defining $\theta = 0$.

In our studies, we found that elementary dislocations were more common (approximately 10 times more prevalent than multiple dislocations). However, single dislocations proved to be difficult to analyze because the absolute magnitude of the distortion was smaller. We found that a radius of 5*b* was the

optimum distance where we could obtain a reasonable number of measurements as a function of azimuthal angle around the dislocation, given our measurement error. For the imaging conditions used here, we could reliably measure the local amount of tilt to within ± 0.5° (Figure 7). This was determined by the limited contrast and inherently noisy low dose HREM images. With samples having higher *d*-spacings and less sensitivity to beam damage (such as block copolymers), it should be possible to obtain better images where smaller amounts of distortion could be measured more accurately and reliably. At larger distances, we encountered distortions due to neighboring defects.

Modulus Calculations. The complete elastic compliance and stiffness matrices of DCHD were required to predict the anisotropic behavior of the dislocation strain field. These moduli were calculated using the elastica module of Polygraf.[32] The procedure was to minimize the energy of the unit cell of the DCHD monomer[33] and polymer[31] to an RMS value of 0.01 kcal/mol by conjugate-gradient methods using the Dreiding II force field.[34] The minimized unit cell energies were 84.3 kcal/mol for the monomer and 153.0 kcal/mol for the polymer. Polygraf calculates the stiffness matrix, c_{ij}, from the second derivative of the energy, U, by:

$$c_{ij} = \frac{\partial^2 U}{\partial \epsilon_i \partial \epsilon_j} \tag{1}$$

where ϵ_i (i=1, 6) is the strain. The compliance matrix is calculated as the inverse of the stiffness matrix. Young's modulus values and isotropic Lamé constants, λ and μ, are calculated as follows:[32]

$$E_x = \frac{1}{s_{11}} \tag{2}$$

$$E_y = \frac{1}{s_{22}} \tag{3}$$

$$E_z = \frac{1}{s_{33}} \tag{4}$$

$$\lambda = {}^1/_3[c_{11} + c_{22} + c_{33}] - {}^2/_3[c_{44} + c_{55} + c_{66}] \tag{5}$$

$$\mu = {}^1/_3[c_{44} + c_{55} + c_{66}] \tag{6}$$

All modulus values are defined relative to the crystal unit cell axes. The crystal compliances, Young's moduli, and Lamé constants for both monomer and polymer DCHD are shown in Table 1. Due to symmetry, monoclinic elastic matrices have 13 independent constants, with all other values being zero.[35] The calculation by Polygraf correctly predicted the placement of the zeros in the stiffness matrix to two significant digits both with and without the symmetry constraints available in the software.

Theories of Distortions around Dislocations. In the following sections, we discuss the theoretically expected distortions around an edge dislocation in an isotropic crystal, an anisotropic crystal, and a columnar liquid crystal. We pay particular attention to the influence of elastic anisotropy on the axial correlations between laterally associated chains.

Dislocations in Solids. Dislocations correspond to linear defects in the translational symmetry of a condensed phase. A displacement field is defined by comparing the coordinates of a distorted material relative to some reference state. The closure failure of a path integral of the displacement field around a dislocation line defines the magnitude and direction of the Burger's vector of the defect.[36] When the Burger's vector is perpendicular to the dislocation line, the defect is an edge dislocation. An edge dislocation can often (but not necessarily always) be envisioned as an extra half-plane of atoms or molecules inserted into a crystal. In the case where the Burger's vector is perpendicular to the chain axis of a polymer crystal, this would result in a plane of chain ends incorporated into the crystal structure. The strain fields around a dislocation line are determined by a two-dimensional set of displacements, u and v, that satisfy the equations of equilibrium and compatibility along with boundary conditions. The strains are calculated by taking the derivatives of the displacements, and the stresses are found from linear elastic theory in which there is a direct proportionality between the stress and strain tensors:

Table 1. Elastic Modulus Determination by Molecular Mechanics Simulations

Monomer

Elastic Stiffness Constants: c_{ij} (GPa)

11.6	11.3	8.9	0	0	0.4
11.3	15.4	11.3	0	0	0.6
8.9	11.3	11.8	0	0	1.1
0	0	0	4.8	2.1	0
0	0	0	2.1	3.3	0
0.4	0.6	1.1	0	0	6.9

Young's Modulus (GPa)

X	3.2
Y	3.1
Z	3.4

Lamé Constants (GPa)

λ	2.9
μ	5.0

Polymer

Elastic Stiffness Constants: c_{ij} (GPa)

20.2	11.8	9.6	0	0	−2.7
11.8	13.5	12.9	0	0	4.2
9.6	12.9	81.7	0	0	6.2
0	0	0	11.9	8.7	0
0	0	0	8.7	13.0	0
−2.7	4.2	6.2	0	0	6.2

Young's Modulus (GPa)

X	1.5
Y	0.9
Z	67.5

Lamé Constants (GPa)

λ	17.7
μ	10.4

$$\sigma_{ij} = c_{ijkl}\epsilon_{kl} \tag{7}$$

The equations of equilibrium require that there be no net forces acting on the body when the dislocation is present. They are formulated from the force−mass−acceleration relationship:

$$0 = \rho\frac{\partial^2 u_i}{\partial t^2} = \frac{\partial \sigma_{ij}}{\partial x_i} \tag{8}$$

When the body is at rest, the acceleration term is zero. The compatibility equations relate the six strain components, since they are all derived from the three displacements:

$$\frac{\partial^2 \epsilon_{ii}}{\partial x_j^2} + \frac{\partial^2 \epsilon_{jj}}{\partial x_i^2} = \frac{\partial^2 \epsilon_{ij}}{\partial x_i \partial x_j} \tag{9}$$

From these equations, it is possible to calculate the strain field around a dislocation as discussed in the following sections and in the appendix. We are particularly interested in evaluating the shear strain in the $x-y$ plane near the dislocation core. The tilt of the unit cell corresponds to shear strain in the $x-y$ plane (Figure 1). With no shear strain, the chain axis will be uniformly oriented. Measurements of the chain tilt therefore provide a direct measure of this shear deformation. Furthemore, since the HREM technique always provides an image which is a projection of the sample structure in the direction of the electron beam, we have implicitly neglected any the variations in the displacement field along the beam direction.

Isotropic Crystal Theory. In an isotropic medium, the elastic response is the same in all directions and the compliance matrix can be described by two Lamé constants, λ and μ.

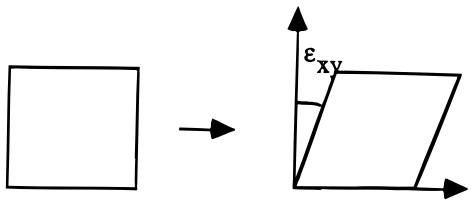

Figure 1. The tilting of molecules originally oriented parallel to the *y*-axis gives an estimate of shear distortions in the $x-y$ plane.

The shear strain around an edge dislocation in a isotropic medium with line vector ξ = [010] and Burgers vector b parallel to [100] is given by:[37]

$$\epsilon_{xy} = \frac{b}{2\pi(1-\nu)} \frac{x(x^2-y^2)}{(x^2+y^2)^2} \tag{10}$$

where b is the Burger's vector, ν is Poisson's ratio, and x and y are coordinates along the [100] and [010] directions, respectively. Poisson's ratio is related to the Lamé constants by:

$$\nu = \frac{\lambda}{2(\mu+\lambda)} \tag{11}$$

The theoretical shear strain field of an edge dislocation in an isotropic medium is shown in Figure 2. The tilt can be plotted as a function of angular position, ϕ, around the dislocation at a constant radius, r. The dislocation is oriented so that the Burger's vector is parallel to the *x*-axis, with the extra half-plane of chains along the positive *y*-axis. The tilt is plotted from as a function of ϕ from 180° to −180°. Examination of the strain field and tilt plots shows that the tilt is highest along the direction of the Burger's vector, tilting to the right on the right of the dislocation ($\phi = 0$) and to the left at $\phi = 180°$. There are reversals of tilt at ±90° which indicate the fact that the planes parallel to *z* are capable of exerting shear strains upon one another. The shear deformation of the planes parallel to *z* arises from the finite values of the compliances c_{44} and c_{55}. The magnitude of the reversals of tilt due to this shear near ± 90° is one-third that of the maximum tilt observed parallel to **b**. This is the characteristic we will focus on when analyzing the behavior of dislocations in anisotropic crystals and columnar liquid crystals.

Anisotropic Crystal Theory. Anisotropic linear elastic dislocation theory has been described by Steeds.[25] The solution of the stress and strain fields involves the compatibility equation method. The boundary conditions for an infinite elastic medium result in a sextic equation for which the solution for the roots comprises the essential problem in anisotropic theory. For certain cases of high symmetry, analytic solutions are available.[25] The symmetry of chain end edge dislocations in DCHD conforms to one of these solutions. The configuration of two types of chain end dislocations possible in DCHD (with b = [100] and b = [010]) is shown in Figure 3. Both have the dislocation line perpendicular to a dyad axis of symmetry in the crystal. This solution also applies to many of the dislocation slip systems in cubic materials. The appendix describes the process and calculations necessary to derive the tilt of the unit cell (shear strain) from the monoclinic stiffness matrix for DCHD monomer and polymer. The calculations reveal that as the anisotropy of the crystal increases, the magnitude of the tilt parallel to b decreases, and the amount of reversal of tilt due to shear correlations between columns decreases.

Columnar Liquid Crystal Theory. Two types of edge dislocations can be defined in columnar liquid crystal systems, a transverse and a longitudinal dislocation. The transverse case occurs when the dislocation line is perpendicular to the column axis, whereas in the longitudinal case they are parallel. The transverse geometry is analogous to chain-end dislocations in crystalline polymers with the Burger's vector perpendicular to the chain axis. In liquid crystals,[28,29] the distortion of the columns around an edge dislocation is derived in terms of a characteristic length, λ_3. λ_3 is defined as the square root of the splay modulus over a combination of two elastic moduli for columnar phases:

$$\lambda_3 = \left(\frac{K_3}{B+C}\right)^{1/2} \tag{12}$$

where K_3 is the splay modulus (with units of energy/length) and B and C are bulk moduli corresponding to column dilatation and column shear, respectively (with units of energy/length^3).

The Burger's vector of a columnar liquid crystal dislocation is defined as the integral of the local normal to the layers, n, around the dislocation core (Figure 4). The distortions include both the tilt and dilation between column layers. The dilation of the layers is:

$$M_x = \frac{-xna_0}{8(\pi\lambda_3)^{1/2}|x|^{1/3}} \exp(-y^2/4\lambda_3|x|) \tag{13}$$

where n is the strength of the Burger's vector and a_o is the layer thickness in the undistorted material. The tilt of the layers is:

$$M_y = \frac{\pm na_0}{4(\pi\lambda_3|x|)^{1/2}} \exp(-y^2/4\lambda_3|x|) \tag{14}$$

where the angle of tilt is defined as the arcsin of the tilt vector, M_y:

$$\theta_{\text{tilt}} = \arcsin(M_y) \tag{15}$$

These distortions are predominantly confined to parabolas along the *x*-axis defined by $y^2 = 4\lambda x$ and decrease rapidly along *y*. This distortion is shown in Figure 5 along with the corresponding tilt diagram. Unlike the isotropic solution for the tilt (Figure 2), the small lobes at ±90° which represent intercolumn shear are not present in the liquid crystal solution. This is because there are no correlations between columns (i.e., c_{44} and c_{55} are zero in the columnar liquid crystal case). Hence, the reversals of tilt due to the shear between planes parallel to *z* seen in isotropic crystals are absent in the liquid crystals.

Hence, we find that the distortions near an edge dislocation in an anisotropic crystal depend upon the relative magnitude of the components of the stiffness matrix. As the anisotropy of the crystal increases, the distortions evolve from the isotropic solution toward the columnar liquid crystal solution.

Both isotropic linear elasticity and columnar liquid crystal theory form extremes for the expected distortion near an edge dislocation. It is reasonable to suggest that the anisotropic elasticity solution would be similar to the isotropic solution at small deviations from the isotropic state, but would tend toward the columnar solution in cases of extreme anisotropic behavior. By measuring the distortions near the dislocation core experimentally, it is possible to estimate the degree of anisotropy of the polymer crystal.

Results and Discussion

Figure 6 is a HREM image of a DCHD three chain-end edge dislocation with a Burger's vector of **b** = 3*a*/2 [100] (2.4 nm). For this dislocation the line vector and Burger's vector are both perpendicular to the covalently bonded chain axis. The fringes are each 0.8 nm in spacing, corresponding to the (200) planes. The procedure was to measure the local tilt of the layer away from its perfect orientation at a constant radius around the dislocation core. This procedure is similar to that used by Hudson et al.[18,19] to map the orientation of the molecular director around a disclination. The tilt at a radius of 5**b** was measured around the dislocation and is shown in Figure 7. We found a maximum tilt

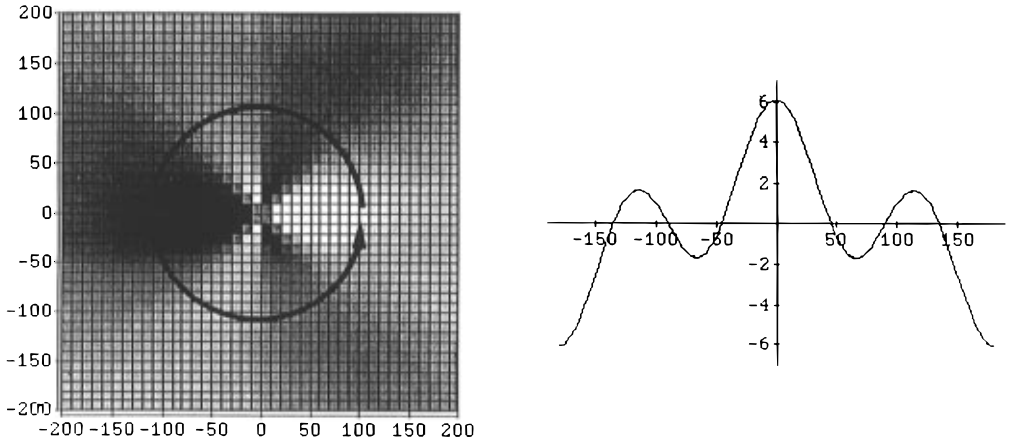

Figure 2. (a, Left) The shear strain around an isotropic edge dislocation where the extra half-plane is oriented along the positive *y*-axis. (b, Right) Magnitude of the tilt (in degrees) as a function of azimuthal angle (in degrees) at a fixed distance (5*b*) from the dislocation core. The large lobes with maxima at 0° and 180° are produced by the tilt of the layers incorporating the extra planes. The smaller lobes are the effect of shear in the *x* direction between individual repeat units along the *y* direction.

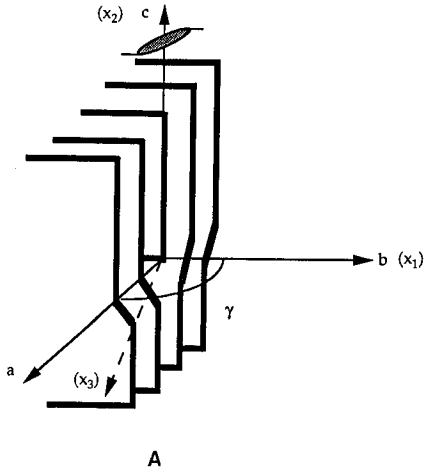

A

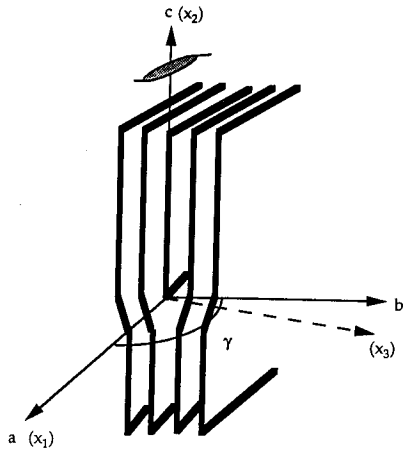

B

Figure 3. Orientations of the two types of chain-end edge dislocations in poly(DCHD). The *a*, *b*, and *c*-axes refer to the unit cell axis system, whereas x_1, x_2, and x_3 are the orthogonal dislocation coordinate system required for strain field calculations using anisotropic dislocation theory.[25] The dyad axis of the space group ($P2_1/c$) is along the *c*-axis and perpendicular to the dislocation lines.

distortion of ±6° at a distance of 12 nm from the core along the direction of the Burger's vector **b**. There are several nearby dislocations evident in Figure 6 which also influence the observed distortion. In particular, we believe that these defects give rise to the asymmetry of

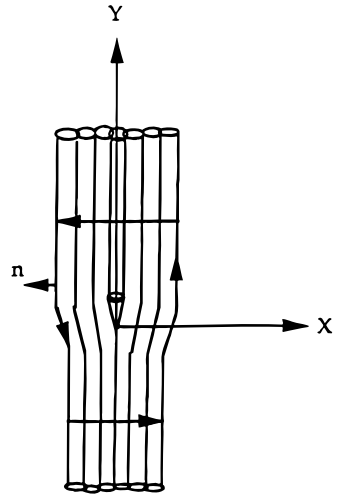

Figure 4. Burger's circuit for a transverse edge dislocation in a columnar liquid crystal.[29]

tilt about $\phi = 0$.

Covalent bonding in the chain direction influences several elements of the elastic stiffness matrix. An examination of the stiffness matrix by expanding the contracted notation[35] shows which terms will be affected by the covalent bonds. For example, the component c_{3321} (c_{36}) relates the strain of the chain in the *x* direction to the normal stress in the chain direction. During the polymerization of diacetylenes, the magnitudes of these stiffness components increase as extended covalent bonding along the chain is established.

We define here an anisotropy parameter, *W*, which is a ratio of stiffnesses dependent on *c*-axis bonding to all other terms. The equation is derived for monoclinic materials but could easily be adapted for polymer crystals of other symmetries.

$$W \equiv \frac{c_{33} + c_{36} + c_{44} + c_{45} + c_{55}}{c_{11} + c_{12} + c_{13} + c_{16} + c_{22} + c_{23} + c_{26} + c_{66}} \qquad (16)$$

For DCHD monomer and polymer elastic stiffnesses calculated from molecular mechanics, *W* is 0.35 and 1.6, respectively. For isotropic materials, *W* reduces to:

$$W = \frac{2c_{11} - c_{12}}{2.5(c_{11} + c_{12})} = \frac{\lambda + 4\mu}{5\lambda + 5\mu} \qquad (17)$$

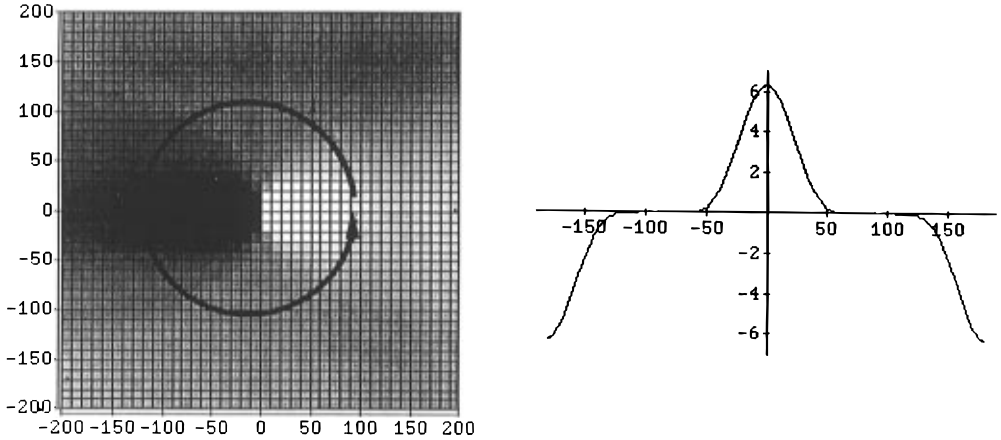

Figure 5. (a, Left) The shear strain around a columnar liquid crystal edge dislocation where the extra half-plane is oriented along the positive *y*-axis. (b, Right) Magnitude of the tilt (in degrees) as a function of azimuthal angle (in degrees) at a fixed distance (5*b*) from the dislocation core. The large lobes with maxima at 0° and 180° are produced by the tilt of the layers due to the extra half-plane of columns. Notice the lack of smaller lobes near ±90° as seen in the isotropic elasticity case (Figure 2b). In the liquid crystal the shear deformation between the columns is suppressed.

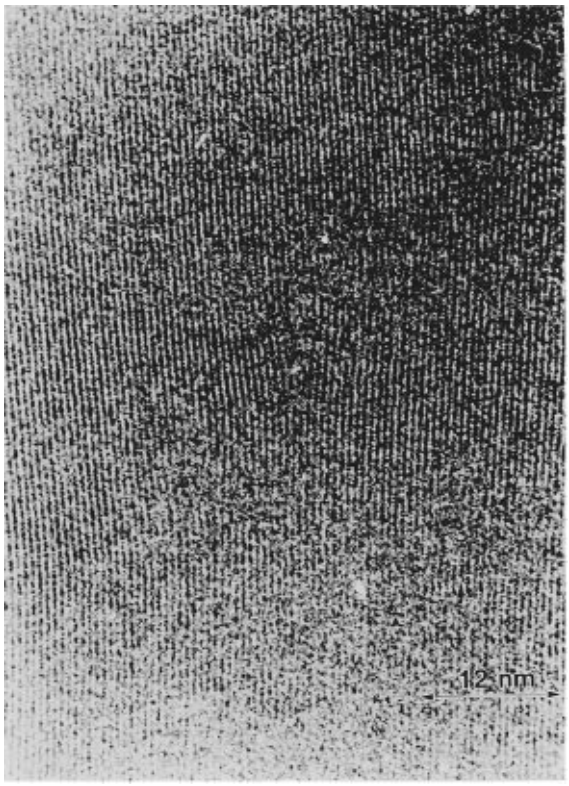

Figure 6. HREM image of a poly(DCHD) three chain-end edge dislocation with Burger's vector 3*a*/2 [100]. The 0.8 nm (200) lattice fringes correspond to the diacetylene chain axis.

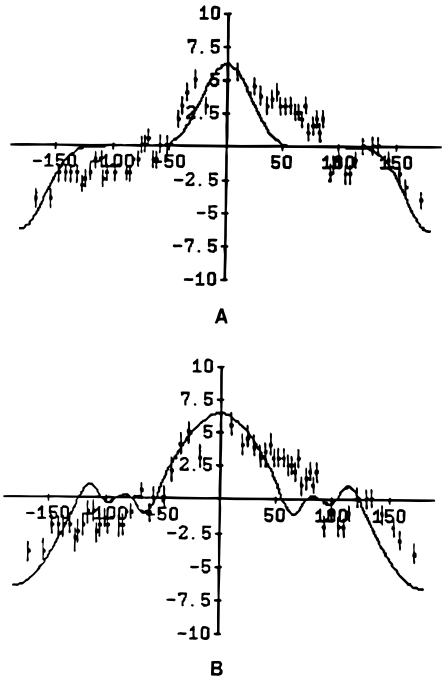

Figure 7. The experimental tilt measured from the HREM image of a three chain-end edge dislocation (Figure 6). The tilt was measured with an error of ±0.5°. (A) shows the experimental data compared to the prediction from columnar liquid crystal theory using a value of $\lambda_3 = 0.8 \pm 0.1$ nm. (B) shows the experimental data compared to the anisotropic linear elastic solution with a polymer anisotropy parameter $W = 3.5$.

As a ratio between different components of the compliance matrix, it is similar in form to other parameters that have been derived to examine anisotropic crystals, such as $A = 2c_{44}/(c_{11} - c_{22})$ and $N = c_{12}/(c_{11} + c_{12})$.[25] Here, our intent is to use W as a means to examine the anisotropy in extended-chain crystalline polymers. The manner in which this parameter varies with the nature and degree of elastic anisotropy, and its utility for describing the transitions to systems with different symmetries, remains to be established. Whether any single parameter will prove to be useful for this endeavor is not yet clear, since the required symmetry breaking might conceivably occur by a number of different mechanisms and in different directions. We are not aware of any extant theoretical approach that provides a measure of the extent of anisotropy during phase transitions from an isotropic crystal to an anisotropic crystal to a liquid crystal.

Using the monomer stiffnesses for c_{11} and c_{12} gives a W parameter of 0.2. Although the moduli calculated from molecular mechanics predicted an anisotropy of 1.6 for the polymer, the experimental data required a value of 3.5 for the best fit. The simulations overestimate the chain modulus and underestimate the transverse modulus when compared to values determined experimentally (45 ± 2 GPa for c_{33}).[38]

During our analysis we found that it was the ratio between the various compliance components, as represented by the parameter W, that primarily determined the predicted distortions near the dislocation core. This result is similar to that of Hudson and Thomas,[18] who

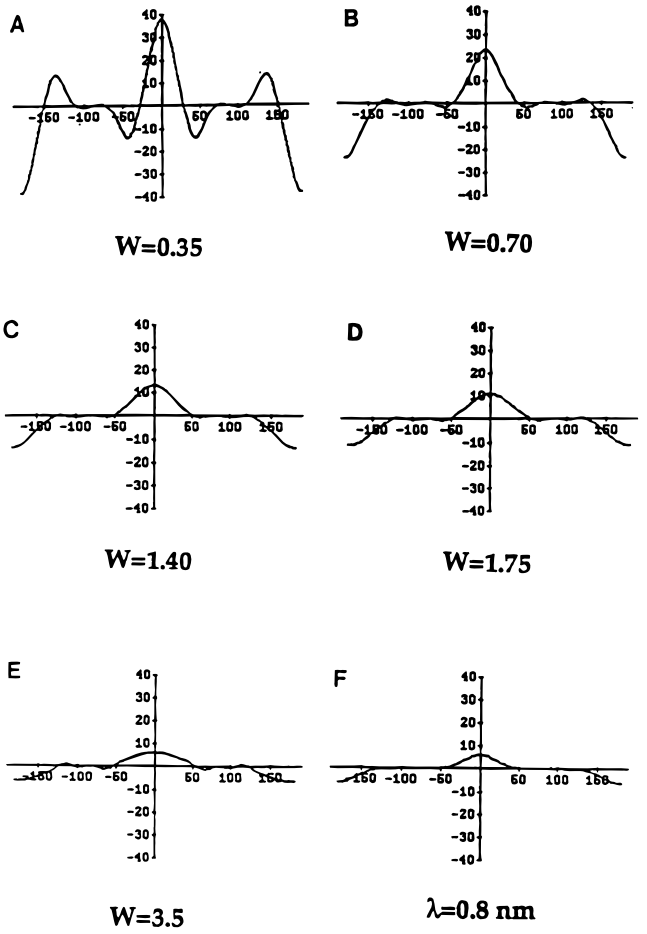

Figure 8. Behavior of the tilt around a three chain-end edge dislocation (in degrees) as predicted by anisotropic linear elasticity for values of $W = 0.35-3.5$ (A-E). (F) shows the corresponding solution provided by columnar liquid crystal theory with $\lambda_3 = 0.8$ nm. As the anisotropy parameter W increases, the magnitude of the tilt at 0° and 180° decreases. The width of the major tilt distortion increases also. The small lobes are suppressed as the anisotropy is more pronounced until they take a value close to zero, approaching the columnar liquid crystal solution.

found that the distortions near disclinations were a function of the ratio between the splay and bend elastic constants, not their absolute magnitudes.

Figure 8 shows the predicted behavior of the tilt around a chain-end edge dislocation as a function of the elastic anisotropy measured by W. The peaks at 50° and 130° are a result of the shearing of individual repeat units of the chain in the x direction. As the moduli increase due to the covalent bonding in the c-direction, the ability of the repeat units in the chain to support shear relative to one other decreases. This results in the suppression of the subsidiary lobes in the plot of ϵ_{xy}. The absolute magnitude of the tilt in the x direction (which is a maximum near 0° and 180°) also decreases. As the anisotropy increases, the tilt becomes similar to that seen in the columnar liquid crystals. The absolute magnitude of the tilt is reduced, and the shearing between chains, evident as a reversal of tilt found between 40° and 150°, is suppressed. As the anisotropy parameter W is increased, the angular width of the region of tilt near 0° and 180° increases.

A plot of the predicted tilt of the theoretical models for the distortion near the dislocation as a function of ϕ and r is shown in Figure 9. The schematics show the tilt of the molecular axis predicted for (a) DCHD monomer using isotropic crystal elasticity, (b) DCHD polymer using anisotropic crystal elasticity ($W = 3.5$), and (c) DCHD polymer using columnar liquid crystal elasticity ($\lambda_3 = 0.8$ nm). The polymer tilt (*b*) for $W = 3.5$ is similar to the columnar liquid crystal solution (*c*), and they both closely resemble the HREM image. It might have been expected that the experimental strain field would be a mixture of the characteristics of both monomer and polymer, since the dislocation was formed in the DCHD monomer first and then polymerized. The data show instead that the dislocation more closely resembles that expected of an anisotropic polymer dislocation.

Our analysis predicts that the distortion of the diacetylene monomer lattice will be spread over a fairly large region near the dislocation core whereas it is localized near the core in the polymer. Dynamic dark-field images recorded during the polymerization by Liao[39] are generally consistent with this finding. Bend contours in the monomer film disappeared as the material polymerized under the effect of the electron beam. Bend contours corresond to a collection of crystal planes which are rotated or bent into the Bragg condition during imaging. The bend contours observed in the monomer correlate to regions of tilt around the dislocation. Upon polymerization, the lattice stiffens and the distortion becomes localized, causing the disappearance of the bend contours.

Near the core of the monomer dislocation, the tilt is predicted to vary greatly from point to point, suggesting that the elastic solution will not remain valid. When the local shear stress exceeds the shear strength of the material, it will plastically deform. Once the material deforms plastically, the elastic solution is no longer applicable. In the monomer diagram (Figure 9A), a circle is drawn at 5**b** from the core. The tilt of the elastic solution for the polymer (Figure 9b,c) changes more uniformly as the dislocation core is approached. This suggests that the core region in the polymer is smaller. Because of the covalent bonding in the y direction, the shear stress to plastically deform the chain in the x direction corresponds to that needed to break the covalent bond. The implication is that anisotropic elastic dislocation theory may be considered valid over most of the area around a polymer chain-end dislocation.

Experiments in our laboratory have measured the photoconductivity of poly(diacetylene)s as a function of bicrystal geometry.[39] At small angles, grain boundaries are expected to be composed of arrays of dislocations. The separation between dislocation decreases with increasing misorientation. The rate at which the photocurrent transport efficiency varies with misorientation angle suggests that the deformation around a dislocation in DCHD poly(diacetylene) is highly localized.

The elastic strain energy for an isotropic dislocation is:

$$E_{\mathrm{el}} = \frac{Gb^2}{4\pi(1-\nu)} \ln(r/r_0) \qquad (18)$$

where R is usually taken as the grain size or cell size ($\sim$1 mm in our case) and r_o is the core radius. For an anisotropic dislocation, the energy takes a similar form:

$$E_{\mathrm{el}} = \frac{K_{ij} b_i b_j}{4\pi} \ln(r/r_0) \qquad (19)$$

where K_{ij} is a factor which takes into account all the moduli (see Appendix). These expressions give esti-

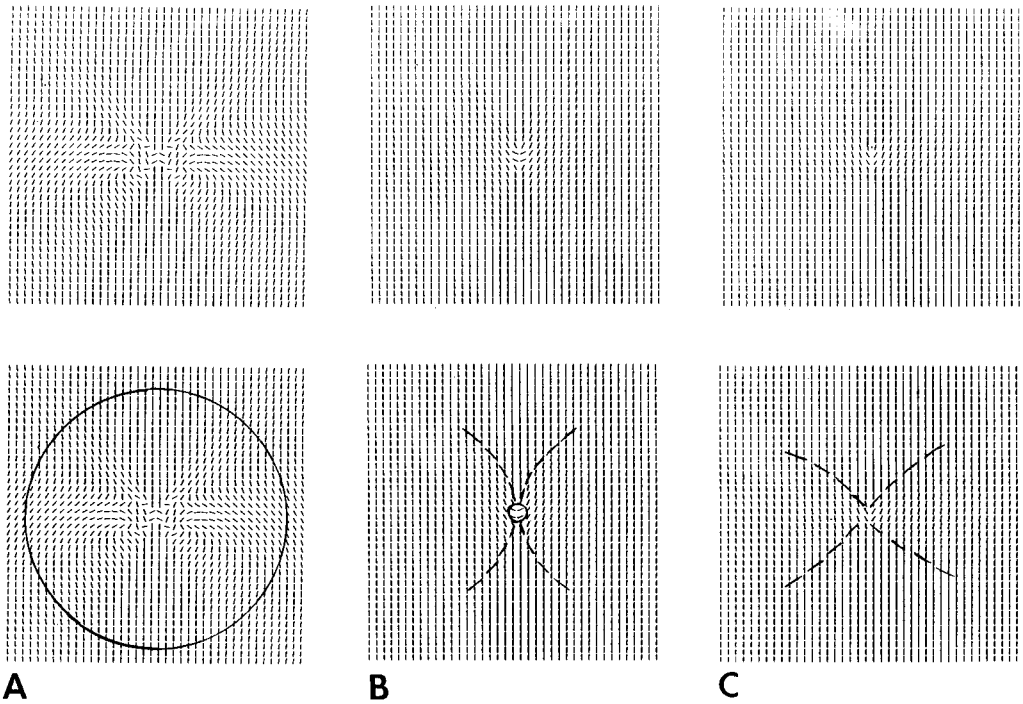

Figure 9. Plots of the local tilt as a function of aziumuthal angle and distance from the dislocation core for the three cases: (a) the monomer anisotropic elastic solution ($W = 0.35$), (b) the polymer anisotropic elastic solution ($W = 3.5$), and (c) the columnar liquid crystal solution ($l = 0.8$ nm). The monomer solution exhibits considerable distortion inside a core radius of $5b$ (circle). The polymer elastic solution is more well-behaved near the dislocation core. Dashed lines define the parabola inside of which the tilt distortion is concentrated. The polymer and columnar solutions both closely resemble the experimental HREM image of a poly(diacetylene) chain-end edge dislocation (Figure 6).

mates of energies in the range of 6×10^{-8} to 20×10^{-8} J/m for dislocations in poly(diacetylene) crystals. These values are higher by 1−2 orders of magnitude than those typically predicted for metallic crystals. This is evidently due to the energy penalty for distorting covalent bonds and the larger dimensions typical of polymer unit cells (large b).

The core energy of a poly(diacetylene) dislocation may be significant due to the altered electronic structure of the chain end. After polymerization, equilibrium hybridization states of carbon atoms near the chain end have not yet been established. During polymerization, it has been found that the poly(diacetylene) chain end structure is dependent on chain length.[40] Below a degree of polymerization of 6, diradicals are seen at the chain ends, whereas in longer chains dicarbenes exist.[41] In the dicarbene a π_z-electron can become delocalized and move along the chain, its position defining the phase boundary between the butatriene and acetylene regions of the chain. This structure may be stable for long chains where the energy gained by the combination of the π_z electron with another at the far end of the chain to form a π bond is offset by the energy required to move the electron over that distance.

In this work we examined the tilt of the chain as revealed by (hk0) fringes which are parallel to the molecular axis. Additional details about the distortions near these defects could be obtained with higher resolution images that resolve (hkl) planes as well. Furthermore, it should also be possible to investigate both the tilt and the dilations of the layers (eqs 13 and 14). This latter study would be easier to accomplish from conventional TEM, SEM, or AFM images of liquid crystalline or microphase separated block copolymers where the layer separation is larger. Finally, future studies could examine the distortions as a function of distance away from the dislocation core, as in the study on disclinations by Hudson et al.[18,19] There are two problems that will arise in this case: (1) at small r, there are only a few lattice lines in any circuit around the defect, and it becomes difficult to collect reliable statistics; and (2) at large r, the interactions between defects become significant, making it difficult to isolate the deformation from an individual dislocation.

Conclusions

The shear strain field around chain-end edge dislocations in the poly(diacetylene) DCHD, which corresponds to the local tilt of the chain axis, has been experimentally quantified from HREM images. Theoretical modeling using linear elastic dislocation theory was used to determine the anisotropy of the elastic moduli. The polymer anisotropy ratio W, defined here as the ratio of stiffnesses dependent on covalent bonds in the chain direction to those unaffected by such bonding, was determined to be $W = 3.5$ for DCHD polymer. By varying the anisotropy, it was found that the shear strain field approached that for a columnar liquid crystal dislocation as the anisotropy increased due to covalent bonding along the chain direction.

The formation of covalent bonds in the chain direction during the polymerization of diacetylene crystals increases the anisotropy of the elastic modulus. This anisotropy was shown to suppress the effect of shear interactions between chains, weakening the axial correlations between laterally associated molecules. As the anisotropy increased, the behavior of the shear strain approached that expected in columnar liquid crystals where the symmetry is such that axial correlations between chains no longer exist.

The uniformity of anisotropic elastic solution near the dislocation suggests that the core is small in these polymer crystals. Dislocation strain energies in the

polymer were found to be higher than comparable dislocations in metals. The electronic structure changes at poly(diacetylene) chain ends may make significant contributions to the core energy and require further study.

Acknowledgment. P.M.W. thanks the AFOSR and NASA for graduate fellowship support. D.C.M. thanks NSF for financial support through Grant DMR-9024876. Support was also provided by the Michigan Memorial Phoenix Project. We would like to thank Prof. Steven D. Hudson at Case Western Reserve University for helpful discussions and suggestions.

Appendix

Procedure to Calculate the Strain Field for a Chain-End Dislocation in an Anisotropic Media. For the DCHD chain end dislocations discussed in this chapter, the following procedure was used to determine the shear strain and tilt around a dislocation. The compliance matrix determined by Polygraf, $\mathbf{s}_{ij}$, is a 6 × 6 matrix in contracted form and referenced to the unit cell (monoclinic) coordinate system. This coordinate system, shown as *a*, *b*, *c* in Figure 3, is not in the correct reference frame to use for anisotropic theory. The derivation uses an orthogonal axis system with the dislocation line parallel to the x_1 axis and the dyad axis of symmetry as x_2. In order to perform the needed transformations of the compliance matrix to the correct coordinate system, the matrix must be in its full 9 × 9 format.

Expansion of the compliance matrix, $\mathbf{s}_{ij}$, to $\mathbf{s}_{ijkl}$ uses the contraction rules (1 = 11, 2 = 22, etc.) as listed by Steeds.[25] The full compliance matrix, $\mathbf{s}_{ijkl}$, is transformed to an orthogonal coordinate system from the monoclinic system by:

$$\mathbf{s}'_{ijkl} = \mathbf{l}_{ip}\mathbf{l}_{jq}\mathbf{l}_{kr}\mathbf{l}_{ls}\mathbf{s}_{pqrs} \tag{20}$$

$$\mathbf{l}_{im} = \cos(\mathbf{x}'_i, \mathbf{x}_m) \tag{21}$$

where $\mathbf{l}_{lm}$ are the direction cosines of new ($\mathbf{x}'_i$) coordinate system relative to the old one ($\mathbf{x}_m$). Summation over the duplicated variables is assumed unless otherwise noted. The $\mathbf{l}_{lm}$ for the experimental situation was:

$$\mathbf{l}_{lm} = \begin{bmatrix} \cos\gamma & 0 & 0 \\ \cos(\pi/2 + \gamma) & 1 & 0 \\ 0 & 0 & 1 \end{bmatrix} \tag{22}$$

A second transformation is necessary to find the stiffness matrix for the dislocation coordinate system outlined above. The direction cosines used were:

$$\mathbf{l}_{lm} = \begin{bmatrix} 1 & 0 & 0 \\ 0 & 0 & 1 \\ 0 & -1 & 0 \end{bmatrix} \tag{23}$$

The resulting compliance matrix (9 × 9) is referenced to the correct coordinate system but must be contracted to the 6 × 6 form, $\mathbf{s}'_{ij}$, via the contraction rules cited before. Since e_{33} will be considered zero, the compliance matrix can be further simplified. A reduced compliance matrix, $\mathbf{S}'_{ij}$, is calculated from $\mathbf{s}'_{ij}$ via:

$$\mathbf{S}'_{lm} = \mathbf{s}'_{lm} - (s'_{3l}s'_{3m}/s'_{33}) \tag{24}$$

The solutions to the differential equation derived from the equations of compatibility are a function of *p*. Solving for p results in a sextic equations which needs to be solved for p_n (1 → 6):

$$p^6 - q_1p^4 + q_2 - q_3 = 0 \tag{25}$$

where

$$q_1 = -\left\{\frac{S'_{11}S'_{44} + S'_{55}(2S'_{12} + S'_{66}) - 2S'_{15}(S'_{25} + S'_{46})}{S'_{11}S'_{55} - S'^{2}_{15}}\right\} \tag{26}$$

$$q_2 = \frac{S'_{22}S'_{55} + S'_{44}(2S'_{12} + S_{'66}) - (S'_{25} + S'_{46})}{S'_{11}S'_{55} - S'^{2}_{15}} \tag{27}$$

$$q_3 = -\frac{S'_{22}S'_{44}}{S'_{11}S'_{55} - S'^{2}_{15}} \tag{28}$$

The roots will occur as pairs of complex conjugates $p_n = p'_n \pm ip''_n$ (n = 1, 2, 3). The roots are chosen so that either:

case a:

$$p_1 = ip''_1$$

$$p_2 = p'_2 + ip''_2$$

$$p_3 = -p'_2 + ip''_2$$

or:

case b:

$$p_1 = ip''_1$$

$$p_2 = ip''_2$$

DCHD monomer and polymer are both case a. The roots found for the theoretical compliance (or stiffness) matrix determined using the Dreiding II force field[34] were:

	monomer	polymer
p_1	$1.5802i$	$0.501663i$
p_2	$0.703452 + 0.656873i$	$0.324411 + 0.377039i$
p_3	$-0.703452 + 0.656873i$	$-0.324411 + 0.377039i$

These roots are in general similar to roots for other materials such as copper, iron, and zinc,[42] the monomer being closer in magnitude to these materials since it is less anisotropic in nature. Several sets of constants are developed as part of the solution to the differential equations:

$$p_3 = ip''_3$$

$$\gamma_n = -\frac{(S'_{15}p_n^2 + S'_{25} + S'_{46})p_n}{S'_4 + S'_{55}p_n^2} \quad \text{(no summation)} \tag{29}$$

$$\mathbf{s} = [s_1, s_2, s_3] = \mathbf{p} \times \mathbf{g} \tag{30}$$

$$D = s_1 + s_2 + s_3 \tag{31}$$

$$B_n(b_1) = -\frac{K_2 b_1}{4\pi D} p_n s_n \quad \text{(no summation)} \tag{32}$$

$$k_2 = \frac{D}{iS'_{22}(s_1/p_1 + s_2/p_2 + s_3/p_3)} \tag{33}$$

$$K_1 = \frac{K_2 {p_n}^2 s_n}{D} \tag{34}$$

K_1 and K_2 are the energy factors used in calculating the energy of a dislocation. The stresses, s_{ij}, are found for each component of the Burger's vector. In our case, $\mathbf{b} = [b_1\ 0\ 0]$, so only terms derived for b_1 are needed:

$$\sigma_{11}(b_1) = \frac{b_1 K_2 x^2}{2\pi D y} \frac{{p_n}^2 s_n}{(x^2 - {p_n}^2 y^2)} - \frac{K_1 b_1}{2\pi y} \tag{35}$$

$$\sigma_{12}(b_1) = \frac{b_1 K_2 x}{2\pi D} \frac{{p_n}^2 s_n}{(x^2 - {p_n}^2 y^2)} \tag{36}$$

$$\sigma_{22}(b_1) = \frac{b_1 K_2 y}{2\pi D} \frac{{p_n}^2 s_n}{(x^2 - {p_n}^2 y^2)} \tag{37}$$

$$\sigma_{13}(b_1) = \frac{b_1 y[x^4 {p_n}^3 \gamma_n s_n + \{q_3 \gamma_n s_n/p_n - q_2 \gamma_n s_n p_n\} x^2 y^2 + p_n \gamma_n s_n q_3 y^4]}{2\pi i S'_{22}(s_m/p_m)(x^6 - q_1 x^4 y^2 + q_2 x^2 y^4 - q_3 y^6)} \tag{38}$$

$$\sigma_{23}(b_1) = \frac{b_1 x[x^4 p_n \gamma_n s_n + \{\gamma_n s_n {p_n}^3 - q_1 \gamma_n s_n p_n\} x^2 y^2 + (\gamma_n s_n/p_n) q_3 y^4]}{2\pi i S'_{22}(s_m/p_m)(x^6 - q_1 x^4 y^2 + q_2 x^2 y^4 - q_3 y^6)} \tag{39}$$

The tilt, ϵ_{12}, is then found from:

$$\epsilon_{ij} = \mathbf{s'}_{ij} \sigma_{ij} \tag{40}$$

References and Notes

(1) Wunderlich, B. *Macromolecular Physics: Crystal Structure, Morphology, Defects*, Academic Press: New York, 1973.
(2) Wunderlich, B.; Kreitmeier, S. N. *MRS Bull.* **1995**, *20* (9), 17.
(3) Reneker, D. H.; Mazur, J. *Polymer* **1983**, *24*, 1387.
(4) Reneker, D. H.; Mazur, J. *Polymer* **1988**, *29*, 3.
(5) Martin, D. C. *Trends Polym. Sci.* **1993**, *1* (6), 178.
(6) Singh, C.; Hone, D. *Bull. Am. Phys. Soc.* **1992**, *37* (1), 315.
(7) Liao, J. Ph. D. Dissertation, The University of Michigan, 1995.
(8) Young, R. J.; Petermann, J. *J. Polym. Sci., Polym. Phys. Ed.* **1982**, *20*, 961.
(9) Wilson, P. M.; Martin, D. C. *J. Mater. Res.* **1992**, *7* (11), 3150.
(10) Schultz, J. *Polymer Materials Science*, Prentice-Hall: Englewood Cliffs, NJ, 1974.
(11) Young, R. J. *Mater. Forum* **1988**, *11*, 210.
(12) Crist, B.; Fisher, C. J.; Howard, P. R. *Macromolecules* **1989**, *22*, 1709.
(13) Read, R. T.; Young, R. J. *J. Mater. Sci.* **1984**, *19*, 327.
(14) Martin, D. C. Ph.D. Dissertation, The University of Massachusetts at Amherst, 1990.
(15) Voigt-Martin, I. G.; Garbella, R. W.; Schumacher, M. *Macromolecules* **1992**, *25*, 961.
(16) Zhang, W.; Thomas, E. L. *Polym. Commun.* **1992**, *32* (16), 481.
(17) Liao, J.; Martin, D. C. *Science* **1993**, *260*, 1489.
(18) Hudson, S. D.; Thomas, E. L. *Phys. Rev. Lett.* **1989**, *62* (17), 1993.
(19) Hudson, S. D.; Fleming, J. W.; Gholz, E.; Thomas, E. L. *Macromolecules* **1993**, *26*, 1270.
(20) Ding, D.; Thomas, E. L. *Macromolecules* **1993**, *26*, 6531.
(21) Corleto, C. R.; Bradley, W. L.; Brinson, H. F. Submitted to *J. Mater. Sci.*
(22) Tsai, K. H.; Schwartzman, A. F.; Gallego, R.; Ortiz, M.; O'Keefe, M. A.; Kim, K. S. *Proc. 50th Annual Meeting of the Electron Microscopy Society of America* **1992**, 144.
(23) Choi, H. C.; Schwartzman, A. F.; Kim, K. S. *Mater. Res. Soc. Symp. Proc.* **1991**, *239*, 419.
(24) Pradere, P.; Thomas, E. L. *Ultramicroscopy* **1990**, *32*, 149.
(25) Steeds, J. W. *Introduction to Anisotropic Elasticity Theory of Dislocations*, Clarendon Press: Oxford, 1973.
(26) Peterson, J. M.; Lindenmeyer, P. H. *J. Appl. Phys.* **1966**, *37* (11), 4051.
(27) Thomas, E. L.; Sass, S. L. *Makromol. Chem.* **1973**, *164*, 333..
(28) Kléman, M.; Oswald, P. *J. Phys.* **1982**, *43*, 655.
(29) de Gennes, P. G; Prost, J. *The Physics of Liquid Crystals, 2nd ed.*, Clarendon Press: Oxford, 1993.
(30) Wilson, P. M.; Martin, D. C. *J. Mater. Res.* **1992**, *7* (11), 3150.
(31) Apgar, P. A.; Yee, K. C. *Acta Crystallogr.* **1978**, *B34*, 957.
(32) Molecular Simulations, Inc., PolyGraf version 3.2, 1992.
(33) Enkelmann, V.; Schleier, G.; Wegner, G.; Eichele, H.; Schwoerer, M. *Chem. Phys. Lett.* **1977**, *52* (2), 314.
(34) Mayo, S. L.; Olafson, B. D.; Goddard, W. A. *J. Phys. Chem.* **1990**, *94*, 8897.
(35) Nye, J. F. *Physical Properties of Crystals*, Clarendon Press: Oxford, 1957.
(36) Hirth, J. P.; Lothe, J. *Theory of Dislocations, 2nd ed.*, John Wiley and Sons: New York, 1982.
(37) Hull, D.; Bacon, D. J. *Introduction to Dislocations, 3rd ed.*, Pergamon Press: Oxford, 1984.
(38) Galiotis, C.; Read, R. T.; Yeung, P. H. J.; Young, R. J. *J. Polym. Sci., Polym. Phys. Ed.* **1984**, *22*, 1589.
(39) Liao, J. Ph.D. Dissertation, The University of Michigan, 1995.
(40) Wright, J. D. *Molecular Crystals*, Cambridge University Press, Cambridge, 1987.
(41) Huber, R.; Schwoerer, M.; Bubek, C.; Sixl, H. *Chem. Phys. Lett.* **1978**, *53*, 35.
(42) Teodosiu, C. *Elastic Models of Crystal Defects*; Springer-Verlag: New York, 1982.

MA9506748